

Multi-energy diffuse neutrino fluxes originating from core-collapse supernovae

Yosuke Ashida^{1,*}

¹*Department of Physics and Astronomy, University of Utah, Salt Lake City, Utah 84112, USA*

(Dated: January 24, 2024)

A comprehensive framework is proposed for the diffuse neutrino fluxes attributed to two different physical processes in core collapse of massive stars. In this scheme, models of thermal MeV-scale neutrinos produced at the core of collapsing stars and non-thermal high-energy neutrinos emitted from accelerated cosmic rays interacting with circumstellar material are bridged through features of core-collapse supernovae (progenitor mass and optical properties). The calculated diffuse fluxes are presented with discussion about their detection prospects at neutrino telescopes.

I. INTRODUCTION

Massive stars are known to undergo a fierce fate at the end of their life; their self-gravity surpasses pressures with nuclear fusion at the final stage of stellar evolution and the following shock wave produced by the nuclear repulsion force (core bounce) propagates outwards to blow off the stellar envelope (e.g., see Refs. [1, 2] for more details). This is called core-collapse supernovae (CCSNe) and expected for stars with masses of $\gtrsim 8M_{\odot}$. Throughout the core-collapse process, *thermal* neutrinos of all flavors are expected to be produced, e.g., via electron capture and pair annihilation (see Ref. [3–5] for recent reviews). Such neutrinos are believed to be a key for successful explosions as they could prevent momentum of the shock wave from diluting before reaching the stellar surface. These thermal neutrinos from the star’s core are emitted up to a timescale of $O(10)$ s from the core bounce and their typical energy scale is $O(1\text{--}10)$ MeV [6–9]. Although there have been huge efforts made on the theoretical side for deeper understanding of the CCSN mechanism both numerically and analytically, a complete picture of the collapsing process is still awaited. On the experimental side, there has been only one successful observation of supernova neutrinos, which is SN 1987A in the Large Magellanic Cloud [10–12].

Further neutrino emission from CCSNe is expected at later times with a much longer timescale, $O(1)$ hour to $O(1)$ year, due to confined dense circumstellar material (CSM). CSM is predicted to originate from mass loss that massive stars experience 0.1–100 years ahead of core collapse [13–16] and its existence is strongly supported by recent optical observations of supernovae [17–25]. Likely processes that cause the star’s mass loss are stellar winds and interactions between binary stars [26, 27]. The supernova ejecta interacts with the surrounding CSM, accelerating charged particles therein to relativistic energies via the Fermi shock acceleration process [28–30]. These relativistic particles then interact with non-relativistic particles (pp collisions) to produce charged mesons that decay into neutrinos, e.g., $pp \rightarrow \pi^+ \rightarrow \mu^+\nu_{\mu} \rightarrow$

$e^+\nu_e\bar{\nu}_{\mu}\nu_{\mu}$ [31–39]. Energies of neutrinos from such *non-thermal* process are expected to reach $O(10^4\text{--}10^6)$ GeV depending on the CSM feature etc. Emission timescale, $O(1)$ hour to $O(1)$ year, is determined by the ejecta velocity and CSM density profile. Detection of non-thermal supernova neutrinos has never been confirmed, though several studies investigate potential detection at multiple experiments in the future [40–42].

Measuring the accumulated flux of supernova neutrinos released over the cosmic history serves another direction of probing the supernova feature. In contrast to detecting neutrinos from a transient source, such methodology is useful for acquiring more general and average picture and holds a merit of not requiring to wait for another nearby supernova. The integrated flux of thermal neutrinos is referred to as the diffuse supernova neutrino background (DSNB), or supernova relic neutrinos (SRNs) in some articles, and still remains undiscovered in spite of intensive searches at neutrino detectors around the world, such as Super-Kamiokande and KamLAND [43–45] (e.g., Refs. [46, 47] provide reviews of recent progress in theoretical and experimental DSNB studies). In the high-energy regime, the diffuse neutrino flux of astrophysical-origin beyond the known atmospheric background has been measured by IceCube [48–51]. Their origin is not completely ascertained yet; however, observations of high-energy neutrinos in the direction of some astronomical objects are reported, from the blazar TXS 0506+056 [52] and the active galaxy NGC 1068 [53]. Neutrinos from CCSNe through the inelastic pp process mentioned above may contribute partially to the observed diffuse flux [32–37].

So far, theoretical studies on neutrino emissions from the core and outer region of CCSNe have been made only independently, as tracing physics over the entire dynamics throughout core collapse to ejecta-CSM interactions is quite challenging. Nevertheless, utilizing neutrinos from those two processes by any means should confer benefits for multifaceted comprehension of CCSNe. The scope of this paper is to provide a comprehensive framework for the CCSN-origin diffuse neutrino fluxes in different energy regimes due to two distinctive physical processes. For this purpose, a conventional classification of supernovae based on observed lines and spectral features in the optical survey [54, 55] is referred in conjunction with

* assy.8594.1207.physics@gmail.com

progenitor features, particularly their initial mass.

The rest of this paper is structured as follows. Section II introduces the supernova classification used for the later calculation of the diffuse fluxes and is followed by Section III in which models of thermal MeV neutrinos and non-thermal high-energy neutrinos are described. The calculated neutrino fluxes are presented in Section IV and the results are discussed in more detail in Section V. Finally, concluding remarks are given in Section VI.

II. SUPERNOVA CLASSIFICATION

Supernovae (SNe) are provoked either through a thermonuclear or core-collapse process depending on their mass. Apart from that, they are classified based on their light curves and spectral features in the optical survey [54–56]. The presence of silicon lines indicates a thermonuclear process and SNe with silicon lines are labeled as Type Ia. The others are considered to be based on a core-collapse process. Among them, SNe without hydrogen lines are Type I which are then classified as Type Ib (Ic) if the helium lines are (not) observed. SNe with hydrogen lines are assorted into Type II and further subdivided based on the observed optical properties into II-L, II-P, II*n* and II*b*. SNe Type II-L show a light curve with a steady (“L”)inear decline along the time, while SNe Type II-P retain their brightness at later times (“P”)lateau). SNe Type II*n* show narrow or intermediate hydrogen emission lines (“N”)arrow). SNe Type II*b* have weak hydrogen lines and then resemble Type Ib which do not show hydrogen lines. In the following part of the paper, neutrino emission from CCSNe, i.e., SNe other than Type Ia, is focused.

The observed lines and spectral shapes should reflect stellar envelope and circumstellar environment which are expected to be the outcomes of stellar evolution. Among important factors that determine evolutionary path are star’s mass, metallicity, stellar winds, and binary interactions. For example, SNe Type Ibc (Ib and Ic) are expected to be heavier than Type II, if they are single without a companion star, because of active stripping of the envelope [57]. SNe Type Ic are considered to be heavier than Ib for the same reason. It should be noted that this may differ for binary stars as mass transfer makes the situation more complex [57–59]. The narrow hydrogen lines observed from SNe Type II*n* imply active interactions between the SN ejecta and CSM. In Ref. [57], multiple cases are considered to subdivide the initial mass function (IMF) so that the resulting fractions of CCSN types are consistent with the observation in the Lick Observatory Supernova Search (LOSS). Here, the Salpeter IMF ($\psi_{\text{IMF}} \propto M^{-2.35}$) [60] is adopted and the mass range of 8.5 to $150M_{\odot}$ is assumed for CCSNe. Among multiple scenarios proposed in Ref. [57], the “hybrid #1” scenario (see Figure 7 in that paper) is adopted for the current study. In this scenario, Type II-P, II-L,

II*n*, and roughly half of Ic are considered to arise from single stars and II*b*, Ib, and the remainder of Ic result via binary systems. This scenario has several strengths while no obvious disadvantages. The assigned mass range for II-P ($8.5\text{--}18.7M_{\odot}$) is in a good agreement with the observation and the narrow range for II-L ($18.7\text{--}23.1M_{\odot}$) is also consistent. Most massive single stars die either as II*n* ($23.1\text{--}37M_{\odot}$) or Ic ($37\text{--}150M_{\odot}$). These different fates may be determined by other factors that change the mass-loss efficiency of single stars, such as rotation and metallicity (e.g., Ref. [56] reports that SNe Type II*n* tend to be observed in lower-metallicity galaxies). The binary star case (II*b*, Ib, and partial Ic) is sampled over the entire mass range, $8.5\text{--}150M_{\odot}$, as the mass-loss efficiency is determined not only by the initial mass but also by other factors such as the binary separation for binary stars. This gives a good explanation for the tiny observed difference between Ib and II*b*. For calculating the DSNB flux in Section IV, the progenitor model has to be selected for each SN type. As described in Section III A, models of a progenitor with $15M_{\odot}$ (CNS) and $40M_{\odot}$ (HNS) are used in this study, and either model is assigned to each SN type. The CNS (HNS) model is used for SNe that are mapped as lighter (heavier) than $23.1M_{\odot}$ on the Salpeter IMF, which constitutes 75.7% (24.3%) of total. The consequent fraction of high-mass neutron stars (24.3%) is consistent with the fraction from observations of binary pulsar systems ($\sim 20\%$) [61]. This choice is supported also by other studies that report SNe Type II*n* and Ic are likely to result from very massive stars [62–64], although the potential systematic uncertainty should be noted. The SN type, fraction, original situation, and corresponding progenitor model in this study are summarized in Table I.

TABLE I. SN classification, portion, original situation, and progenitor model used in the present work.

SN type	fraction	origin	progenitor model
II-P	48.2%	single	CNS
II-L	6.4%	single	CNS
II <i>n</i>	8.8%	single	HNS
II <i>b</i>	10.6%	binary	CNS, HNS
Ib	26.0%	binary	CNS, HNS
Ic		single, binary	CNS, HNS

III. NEUTRINO EMISSION

A. Neutrinos from thermal process at stellar core

There are majorly two fates after the star’s core collapse; a *neutron star* (NS) is left after successful blow off of the envelope and cooling of the core (successful SN explosion), or a *black hole* (BH) is formed as continuous mass accretion leads to the critical point (failed SN) (fallback SNe that undergo successful explosions but lead

to the BH formation because of the late-time substantial fallback may exist but are considered to be rare). Neutrinos are expected to be emitted from both cases and their energy spectra are known to differ [7, 65]. However, considering the BH formation requires a modification of the mapping on the Salpeter IMF adopted from Ref. [57] (see Section II). In addition, the fraction of such BH formation case as a function of progenitor mass is not well known. For these reasons, contributions from failed SNe are ignored in the main part of this paper, which does not change the scope of this study, and relevant discussion is given later in Section V. As a model of neutrino emission from the successful explosion that forms a NS, the numerical simulation results from a previous work [66] are adopted, in which two cases on the remaining NS mass (baryonic NS masses of $1.47M_\odot$ and $1.86M_\odot$) are calculated. The corresponding progenitors for these two cases are taken from Ref. [67] and have the solar metallicity with zero-age-main-sequence (ZAMS) masses of $15M_\odot$ and $40M_\odot$, respectively. In the following part, these two models are referred to as the canonical-mass NS (CNS) and high-mass NS (HNS), respectively. As summarized in Table I, the CNS and HNS models are assigned to SNe mapped as lighter and heavier than $23.1M_\odot$ on the Salpeter IMF, respectively.

The neutrino emission profile (total and average energies of emitted neutrinos) depends strongly on the choice of nuclear equation of state (EOS) [66, 68–70]. In the present work, three types of nuclear EOS are considered: LS220 EOS [71], Shen EOS [72], and Togashi EOS [73]. Properties of the remnant NS and the resulting neutrino signal for each EOS case are summarized in Table 1 of Ref. [74]. Detailed neutrino light curves for each case are available in Refs. [65, 66]. In a brief summary, the emitted neutrino amount is largest (smallest) with Togashi (Shen) EOS for both CNS and HNS cases.

B. Neutrinos from pp interactions in outer region

In this study, models from Refs. [34, 39] are adopted for neutrino production from ejecta-CSM interactions. The models are characterized by the CSM density profile, $D r^{-2}$, where r is distance and $D \equiv 5 \times 10^{16} \text{ g cm}^{-1} D_*$ (D is related to the mass-loss rate and wind velocity). D_* differs for each SN type as summarized in Table 1 of Ref. [34]. The most dense CSM ($D_* = 1$) is assumed for SNe Type IIn, while smaller D_* 's are used for the other types ($D_* = 10^{-2}$ for II-P, 10^{-3} for II-L/IIb, and 10^{-5} for Ibc). Here, for II-P, the case with an enhanced CSM motivated by SN 2013fs [18] is used.

Cosmic rays are accelerated by the shock acceleration mechanism similarly to the SN remnants [75]. Such cosmic rays then interact with low-energy nucleons in CSM to produce mesons which are parents of high-energy neutrinos. Here, the cosmic ray spectrum following a power law index of s is considered. The resulting neutrino energies are typically $\sim 5\%$ of the parent proton energy [76].

All neutrino flavors ($\nu_e, \bar{\nu}_e, \nu_\mu, \bar{\nu}_\mu, \nu_\tau, \bar{\nu}_\tau$) are produced equally in the current scenario. The timescale that neutrino emission begins depends on the SN type; $O(1)$ hour for Ibc, II-L, and IIb, $O(1)$ day for II-P, and $O(10)$ day for IIn. Among different SNe, Type IIn gives the largest neutrino flux as its CSM density is highest, and followed by II-P, II-L/IIb, and Ibc in the descending order. Neutrino light curves and fluxes from each SN type are shown in Refs. [34, 39] (e.g., see Figure 2 of Ref. [39]).

IV. DIFFUSE NEUTRINO FLUX

A. Diffuse flux of thermal SN neutrinos (DSNB)

The DSNB flux is calculated by integrating thermal neutrinos from CCSNe over the cosmic history as:

$$\frac{d\phi_{\text{DSNB}}(E_\nu)}{dE_\nu} = c \int_0^{z_{\text{max}}} R_{\text{CC}}(z) \left\langle \frac{dN_{\text{thermal}}(E'_\nu)}{dE'_\nu} \right\rangle \times \frac{dz}{H_0 \sqrt{\Omega_m(1+z)^3 + \Omega_\Lambda}}, \quad (1)$$

where c is the speed of light and $\Omega_m = 0.2726$, $\Omega_\Lambda = 0.7274$, and $H_0 = 70.4 \text{ km s}^{-1}$ are the cosmological constants [77]. The neutrino energy at Earth (E_ν) is related to that at a SN (E'_ν) with a redshift z as $E'_\nu = (1+z)E_\nu$. The integration is performed up to $z_{\text{max}} = 5$ in this study as contributions from $z > 5$ are tiny. The average neutrino number spectrum is obtained by mixing number spectra for each fate ($dN_{\text{CNS}}(E'_\nu)/dE'_\nu$ and $dN_{\text{HNS}}(E'_\nu)/dE'_\nu$) with a fraction of high-mass neutron star cases to all CCSNe (f_{HNS}) as:

$$\left\langle \frac{dN_{\text{thermal}}(E'_\nu)}{dE'_\nu} \right\rangle = f_{\text{HNS}} \frac{dN_{\text{HNS}}(E'_\nu)}{dE'_\nu} + (1 - f_{\text{HNS}}) \frac{dN_{\text{CNS}}(E'_\nu)}{dE'_\nu}. \quad (2)$$

The core-collapse rate $R_{\text{CC}}(z)$ is calculated by utilizing the Illustris-1 cosmological simulation [77, 78] as:

$$R_{\text{CC}}(z) = \dot{\rho}_*(z) \frac{\int_{M_{\text{min}}}^{M_{\text{max}}} \psi_{\text{IMF}}(M) dM}{\int_{0.1M_\odot}^{M_{\text{max}}} M \psi_{\text{IMF}}(M) dM}, \quad (3)$$

where $\dot{\rho}_*(z)$ is the cosmic star formation rate density (SFRD). Here, $M_{\text{min}} = 8.5M_\odot$ and $M_{\text{max}} = 150M_\odot$ and the Chabrier IMF [79], that follows a lognormal function for $M < 1M_\odot$ and a power law with the same slope as the Salpeter IMF (-2.35) for $M > 1M_\odot$, are used. Note that the results are not affected by a different IMF choice between the SN classification in Section II and Eq. (3) as both the Salpeter and Chabrier IMFs are consistent in the mass range for CCSNe ($M > 8.5M_\odot$ in this study). In the present work, the core-collapse rate equals the rate of CCSNe (successful explosions) as the BH formation case is not considered.

In the energy regime of $O(10)$ MeV, the main detection channel of DSNB neutrinos is inverse beta decay of electron antineutrinos ($\bar{\nu}_e + p \rightarrow e^+ + n$) because of the largest cross section [80–82]. Hence, the DSNB flux of $\bar{\nu}_e$ is focused in this study. The $\bar{\nu}_e$ flux at Earth is a mixture of the fluxes of all flavors at production due to the matter effect [83, 84]. The effect of this flavor mixing differs for neutrino mass ordering, *normal* (NMO) or *inverted* (IMO). Both NMO and IMO cases are considered in this study. The resulting $\bar{\nu}_e$ flux at Earth in each neutrino mass ordering case is as follows:

$$\frac{d\phi_{\bar{\nu}_e}}{dE_\nu} \approx 0.68 \times \frac{d\phi_{\bar{\nu}_e}^0}{dE_\nu} + 0.32 \times \frac{d\phi_{\bar{\nu}_x}^0}{dE_\nu} \quad (\text{NMO}), \quad (4)$$

$$\frac{d\phi_{\bar{\nu}_e}}{dE_\nu} \approx \frac{d\phi_{\bar{\nu}_x}^0}{dE_\nu}, \quad (\text{IMO}), \quad (5)$$

where $d\phi_{\bar{\nu}_e}^0/dE_\nu$ and $d\phi_{\bar{\nu}_x}^0/dE_\nu$ are the $\bar{\nu}_e$ and $\bar{\nu}_x$ ($= \bar{\nu}_\mu + \bar{\nu}_\tau$) fluxes at production, respectively. The calculated DSNB $\bar{\nu}_e$ fluxes at Earth for the CNS and HNS cases are shown in Figure 1. Here, the fractional parameter of $f_{\text{HNS}} = 0.24$, a consequence of the mapping of SN types defined in Section II, is used. The results with different nuclear EOS and neutrino mass ordering cases are shown as bands. In the figure, the latest upper limits from Super-Kamiokande [43, 44] and KamLAND [45] are also shown. The current world record is away from the prediction in this study by a factor to ~ 1 order of magnitude around $E_\nu \approx 20$ MeV.

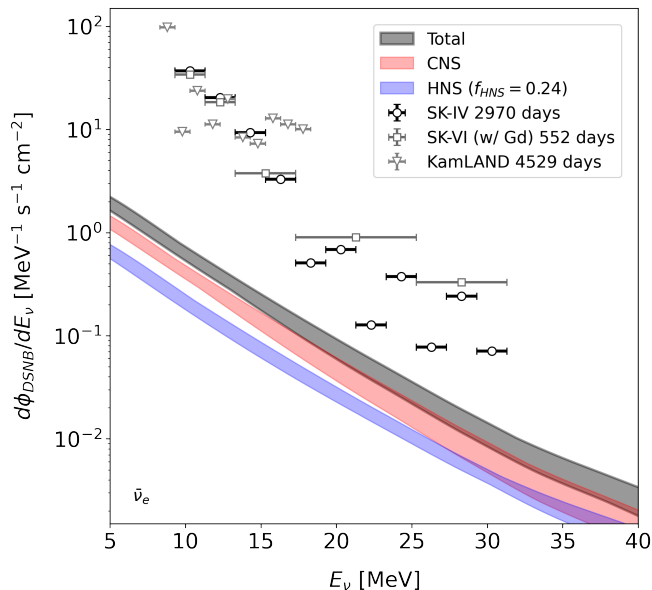


FIG. 1. Calculated DSNB $\bar{\nu}_e$ flux in comparison with experimental upper limits from Super-Kamiokande [43, 44] and KamLAND [45]. Contributions from the CNS and HNS cases with $f_{\text{HNS}} = 0.24$, and their sum are shown. The bands cover different choices of the nuclear EOS (LS220, Shen, or Togashi) and neutrino mass ordering (NMO or IMO).

B. Diffuse flux of non-thermal SN neutrinos

The diffuse flux of SN high-energy neutrinos is calculated similarly to DSNB as:

$$\frac{d\phi_{\text{HE}\nu}(E_\nu)}{dE_\nu} = \frac{c}{4\pi} \int_0^{z_{\text{max}}} R_{\text{CC}}(z) \left\langle \frac{dN_{\text{HE}\nu}(E'_\nu)}{dE'_\nu} \right\rangle \frac{dz}{H_0 \sqrt{\Omega_m(1+z)^3 + \Omega_\Lambda}}, \quad (6)$$

where $R_{\text{CC}}(z)$ is the core-collapse rate calculated in Eq. (3). The same values are used for the cosmological parameters Ω_m , Ω_Λ , H_0 , and z_{max} as in Section IV A. Different from the DSNB energy range, because attenuation of the high-energy neutrino flux due to Earth is significant in the context of detection, the flux per solid angle is more useful. Therefore, a spherical integral over solid angles is not applied (4π in the denominator is its reflection). The average neutrino number spectrum is calculated by summing that from each SN type ($dN_{\text{IIIn}}(E'_\nu)/dE'_\nu$, $dN_{\text{II-P}}(E'_\nu)/dE'_\nu$, $dN_{\text{II-L/IIb}}(E'_\nu)/dE'_\nu$, $dN_{\text{Ibc}}(E'_\nu)/dE'_\nu$) with fractional parameters for each as:

$$\begin{aligned} \left\langle \frac{dN_{\text{HE}\nu}(E'_\nu)}{dE'_\nu} \right\rangle &= f_{\text{IIIn}} \frac{dN_{\text{IIIn}}(E'_\nu)}{dE'_\nu} \\ &+ f_{\text{II-P}} \frac{dN_{\text{II-P}}(E'_\nu)}{dE'_\nu} \\ &+ f_{\text{II-L/IIb}} \frac{dN_{\text{II-L/IIb}}(E'_\nu)}{dE'_\nu} \\ &+ f_{\text{Ibc}} \frac{dN_{\text{Ibc}}(E'_\nu)}{dE'_\nu}, \end{aligned} \quad (7)$$

where $f_{\text{IIIn}} + f_{\text{II-P}} + f_{\text{II-L/IIb}} + f_{\text{Ibc}} = 1$. Here, the sum of all neutrino flavors ($\nu_e + \bar{\nu}_e + \nu_\mu + \bar{\nu}_\mu + \nu_\tau + \bar{\nu}_\tau$) is considered. The resulting diffuse flux is shown in Figure 2 together with the observed astrophysical neutrino flux from a recent analysis using 10 years of IceCube data [85] (the shown fluxes are multiplied by E_ν^2 following the convention in the field). Here, the results with $2.0 \leq s \leq 2.2$ as the spectral index of the original cosmic ray flux are shown as bands. The model prediction from this study can explain 5–10% of the currently observed flux around $E_\nu \approx 10^4$ GeV.

V. DISCUSSION

As shown in Figures 1 and 2, there are some systematic factors that change the fluxes of thermal MeV and non-thermal high-energy neutrinos independently, e.g., the nuclear EOS, neutrino mass ordering, the CSM density profile, and the spectral index of parent cosmic rays in the current study. Therefore, detecting the diffuse neutrino flux at multiple energies enables an access to different aspects of CCSNe, which will give rise to a comprehensive understanding of collapsing massive stars.

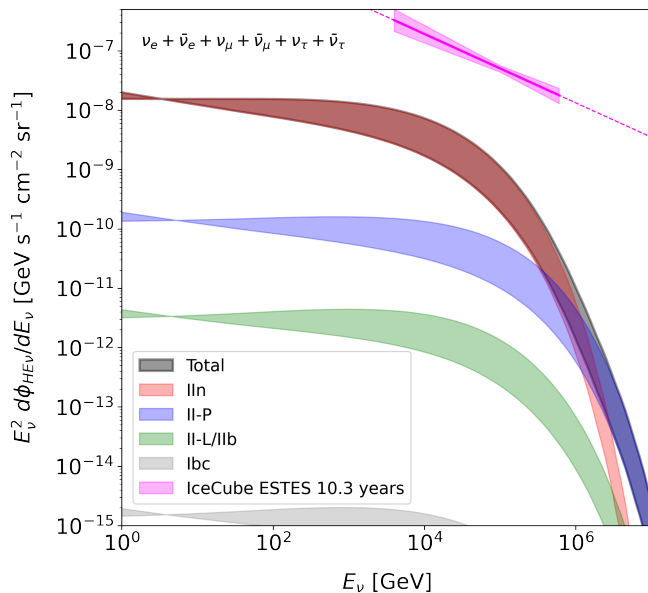


FIG. 2. Calculated diffuse high-energy SN neutrino flux ($\nu_e + \bar{\nu}_e + \nu_\mu + \bar{\nu}_\mu + \nu_\tau + \bar{\nu}_\tau$) in comparison with the measured diffuse astrophysical neutrino flux in a recent IceCube analysis using starting track events (ESTES) [85]. Contributions from each SN type and their sum are shown. The bands cover the different spectral indices of the parent cosmic ray flux ($2.0 \leq s \leq 2.2$).

Not only independent systematic factors, but also there are many more common factors that change the DSNB and high-energy SN neutrino fluxes. SFRD is among the most influential factors as its choice is directly reflected as a scale of the diffuse flux. In Refs. [86, 87], the SFRD impact on the DSNB flux is discussed, where the systematic effect is estimated to be as large as 10–30%. A similar size effect is expected for the diffuse flux of high-energy SN neutrinos. IMF is another important choice which determines the core-collapse rate as seen in Eq. (3). Systematic impacts of the IMF form are discussed in many articles (e.g., see Ref. [88]). Note that switching the IMF form may require mapping of the SN type along progenitor mass proposed in Ref. [57]. In addition, the progenitor fate influenced by binary interactions is recently investigated in a theoretical way [58, 59]. Further progress in such area may advance categorization of the SN type.

In Figures 1 and 2, the BH formation is ignored, but there should be some contributions from such case. A recent search for failed SNe in nearby galaxies shows a fraction of failed SNe to be 4–39% at a 90% confidence level [89]. In Ref. [90], theoretical prediction on the BH fraction is given as 9–32%. A choice of the BH formation fraction (f_{BH}) changes the CCSN rate as $(1 - f_{\text{BH}}) \times R_{\text{CC}}(z)$. This decreases the non-thermal high-energy SN neutrino flux, while the DSNB flux is enhanced at higher energies, especially at $E_\nu \gtrsim 30$ MeV, not only is decreased at lower energies contributed mainly from

the CNS and HNS cases. It should be noted that inclusion of failed SNe in the scheme would change mapping of the SN types on the Salpeter IMF in the high mass region hence impact the resulting diffuse fluxes. The systematic effects on DSNB from the failed SN fraction are investigated in other studies [74, 87, 91].

As mentioned before, a complete modeling of the entire process from core collapse to ejecta-CSM interactions is challenging and not yet performed; however, a bunch of theoretical studies have made huge progress in each physical stage (e.g., see Ref. [4] and references therein). Towards such comprehensive understanding, a long-term modeling of the core-collapse process is essential so that the outcomes of explosions may be available as reliable inputs for the later process that produces high-energy neutrinos. Recently, the late-time phase after core collapse, including proto-NS cooling and fallback mass accretion, are studied in many ways [92–95]. At the same time, because CSM is thought to be formed ahead of the core-collapse process, detailed understanding of stellar evolution of single and binary stars before explosion is also essential [21, 59, 96–98].

Prospects for detecting the diffuse fluxes of SN neutrinos are promising as larger volume and higher performance neutrino telescopes are coming. For the low-energy neutrinos (DSNB), Hyper-Kamiokande [99] is planned as a successor of the on-going Super-Kamiokande detector with a ~ 10 times larger volume and JUNO is being built in China with the best sensitivity expected at lowest energies ($E_\nu \lesssim 10$ MeV) [100–102]. While the astrophysical neutrino flux is detected at IceCube, further precise measurements at IceCube-Gen2 [103] and KM3NeT [104] are expected to help elucidate the neutrino sources, providing some insights into CCSN-origin high-energy neutrinos. These future experiments will play important roles in detecting transient SN sources as well [40, 41, 105–107]. Combining transient and diffuse neutrino measurements will dramatically promote the understanding of SN properties and corresponding theoretical modeling.

VI. CONCLUSION

In this paper, a new comprehensive framework about the diffuse fluxes of SN neutrinos originating from two different physical processes is presented, and the importance of detecting such diffuse neutrino flux at multiple energies is discussed. A conventional SN classification is adopted and the observationally motivated mapping of each type onto the Salpeter IMF for the mass range of $8.5\text{--}150M_\odot$ is referred to bridge between two energy regimes. Models of thermal SN neutrinos based on a progenitor with $15M_\odot$ and $40M_\odot$ are assigned to SNe lighter and heavier than $23.1M_\odot$ on the Salpeter IMF, respectively. In this scheme, SNe Type II-P, II-L, and partial IIb/Ibc are assumed to arise from lighter progenitors, and Type IIn and partial IIb/Ibc are from heavier

ones. Models of neutrino production from ejecta-CSM interactions are taken for high-energy SN neutrinos with different profiles of SN ejecta and CSM being assumed for each SN type (II_n, II-P, II-L/IIb, and Ibc). Both thermal MeV-scale and non-thermal high-energy neutrino fluxes are convoluted with the common cosmological constants and CCSN rate based on the Illustris-1 cosmological simulation and the Chabrier IMF to serve the diffuse fluxes at Earth. The resulting DSNB $\bar{\nu}_e$ flux is close to the current upper limit from Super-Kamiokande within a factor to 1 order of magnitude. The calculated diffuse flux of high-energy SN neutrinos can explain up to $\sim 10\%$ of the currently observed flux of astrophysical neutrinos at Ice-Cube. Note that these fluxes could be further increased or decreased by other systematic factors as discussed in Section V. This work, even though still at a concep-

tual phase, provides a new multifaceted perspective on studying CCSNe via neutrino detection at different energies. Further progress in theoretical studies on the stellar evolution as well as core-collapse process will realize a scheme that unifies two physical processes in a more consistent way.

ACKNOWLEDGMENTS

The author thanks Ken'ichiro Nakazato, Kohta Murase, and Ryo Sawada for fruitful discussions. This work was partially supported by NSF Grant No. PHY-2309967.

-
- [1] K. Kotake, K. Sato, and K. Takahashi, *Reports on Progress in Physics* **69**, 971 (2006), arXiv:astro-ph/0509456 [astro-ph].
 - [2] H.-T. Janka, *Annual Review of Nuclear and Particle Science* **62**, 407 (2012), arXiv:1206.2503 [astro-ph.SR].
 - [3] A. Burrows, *Reviews of Modern Physics* **85**, 245 (2013), arXiv:1210.4921 [astro-ph.SR].
 - [4] I. Tamborra and K. Murase, *Space Science Reviews* **214**, 31 (2018).
 - [5] B. Müller, *Living Reviews in Computational Astrophysics* **6**, 3 (2020), arXiv:2006.05083 [astro-ph.SR].
 - [6] T. Takiwaki, K. Kotake, and Y. Suwa, *Astrophys. J.* **749**, 98 (2012), arXiv:1108.3989 [astro-ph.HE].
 - [7] K. Nakazato *et al.*, *Astrophys. J., Suppl. Ser.* **205**, 2 (2013), arXiv:1210.6841 [astro-ph.HE].
 - [8] Y. Suwa *et al.*, *Astrophys. J.* **881**, 139 (2019), arXiv:1904.09996 [astro-ph.HE].
 - [9] Y. Suwa, A. Harada, K. Nakazato, and K. Sumiyoshi, *Progress of Theoretical and Experimental Physics* **2021**, 013E01 (2021), arXiv:2008.07070 [astro-ph.HE].
 - [10] E. N. Alekseev, L. N. Alekseeva, V. I. Volchenko, and I. V. Krivosheina, *Soviet Journal of Experimental and Theoretical Physics Letters* **45**, 589 (1987).
 - [11] K. Hirata *et al.*, *Phys. Rev. Lett.* **58**, 1490 (1987).
 - [12] R. M. Bionta *et al.*, *Phys. Rev. Lett.* **58**, 1494 (1987).
 - [13] N. Smith, *Annual Review of Astronomy and Astrophysics* **52**, 487 (2014), arXiv:1402.1237 [astro-ph.SR].
 - [14] T. J. Moriya *et al.*, *Mon. Not. R. Astron. Soc.* **439**, 2917 (2014), arXiv:1401.4893 [astro-ph.SR].
 - [15] T. J. Moriya, F. Förster, S.-C. Yoon, G. Gräfenor, and S. I. Blinnikov, *Mon. Not. R. Astron. Soc.* **476**, 2840 (2018), arXiv:1802.07752 [astro-ph.HE].
 - [16] D. Tsuna, K. Kashiwama, and T. Shigeyama, *Astrophys. J.* **914**, 64 (2021), arXiv:2103.08338 [astro-ph.HE].
 - [17] N. Smith, in *Handbook of Supernovae*, edited by A. W. Alsabti and P. Murdin (2017) p. 403.
 - [18] O. Yaron *et al.*, *Nature Physics* **13**, 510 (2017), arXiv:1701.02596 [astro-ph.HE].
 - [19] V. Morozova, A. L. Piro, and S. Valenti, *Astrophys. J.* **858**, 15 (2018), arXiv:1709.04928 [astro-ph.HE].
 - [20] G. Hosseinzadeh *et al.*, *Astrophys. J.* **861**, 63 (2018), arXiv:1801.00015 [astro-ph.HE].
 - [21] F. Förster *et al.*, *Nature Astronomy* **2**, 808 (2018), arXiv:1809.06379 [astro-ph.HE].
 - [22] I. Boian and J. H. Groh, *Mon. Not. R. Astron. Soc.* **496**, 1325 (2020), arXiv:2001.07651 [astro-ph.SR].
 - [23] M. C. Stroh *et al.*, *Astrophys. J. Lett.* **923**, L24 (2021), arXiv:2106.09737 [astro-ph.HE].
 - [24] S. Tinyanont *et al.*, *Mon. Not. R. Astron. Soc.* **512**, 2777 (2022), arXiv:2110.10742 [astro-ph.SR].
 - [25] K. Maeda, in *Handbook of X-ray and Gamma-ray Astrophysics* (2022) p. 75.
 - [26] N. Langer, *Annual Review of Astronomy and Astrophysics* **50**, 107 (2012), arXiv:1206.5443 [astro-ph.SR].
 - [27] F. R. N. Schneider, R. G. Izzard, N. Langer, and S. E. de Mink, *Astrophys. J.* **805**, 20 (2015), arXiv:1504.01735 [astro-ph.SR].
 - [28] S. J. Sturmer, J. G. Skibo, C. D. Dermer, and J. R. Mattox, *Astrophys. J.* **490**, 619 (1997).
 - [29] A. R. Bell, *Brazilian Journal of Physics* **44**, 415 (2014), arXiv:1311.5779 [astro-ph.HE].
 - [30] T. K. Gaisser, R. Engel, and E. Resconi, *Cosmic Rays and Particle Physics* (2016).
 - [31] K. Murase, T. A. Thompson, B. C. Lacki, and J. F. Beacom, *Phys. Rev. D* **84**, 043003 (2011), arXiv:1012.2834 [astro-ph.HE].
 - [32] V. N. Zirakashvili and V. S. Ptuskin, *Astroparticle Physics* **78**, 28 (2016), arXiv:1510.08387 [astro-ph.HE].
 - [33] M. Petropoulou, S. Coenders, G. Vasilopoulos, A. Kamble, and L. Sironi, *Mon. Not. R. Astron. Soc.* **470**, 1881 (2017), arXiv:1705.06752 [astro-ph.HE].
 - [34] K. Murase, *Phys. Rev. D* **97**, 081301 (2018), arXiv:1705.04750 [astro-ph.HE].
 - [35] K. Wang, T.-Q. Huang, and Z. Li, *Astrophys. J.* **872**, 157 (2019), arXiv:1901.05598 [astro-ph.HE].
 - [36] Z. Li, *Science China Physics, Mechanics, and Astronomy* **62**, 959511 (2019), arXiv:1801.04389 [astro-ph.HE].
 - [37] P. Sarmah, S. Chakraborty, I. Tamborra, and K. Auchettl, *Journal of Cosmology and Astroparticle Physics* **2022**, 011 (2022), arXiv:2204.03663 [astro-ph.HE].
 - [38] P. Sarmah, S. Chakraborty, I. Tamborra, and K. Auchettl, *Phys. Rev. D* **108**, 103033 (2023), arXiv:2303.13576 [astro-ph.HE].

- [39] K. Murase, arXiv e-prints , arXiv:2312.17239 (2023), arXiv:2312.17239 [astro-ph.HE].
- [40] N. Valtonen-Mattila and E. O’Sullivan, *Astrophys. J.* **945**, 98 (2023), arXiv:2206.00450 [astro-ph.HE].
- [41] A. Kheirandish and K. Murase, *Astrophys. J. Lett.* **956**, L8 (2023), arXiv:2204.08518 [astro-ph.HE].
- [42] A. Y. Wen, C. A. Argüelles, A. Kheirandish, and K. Murase, arXiv e-prints , arXiv:2309.09771 (2023), arXiv:2309.09771 [hep-ph].
- [43] K. Abe *et al.* (Super-Kamiokande Collaboration), *Phys. Rev. D* **104**, 122002 (2021), arXiv:2109.11174 [astro-ph.HE].
- [44] M. Harada *et al.* (Super-Kamiokande Collaboration), *Astrophys. J. Lett.* **951**, L27 (2023), arXiv:2305.05135 [astro-ph.HE].
- [45] S. Abe *et al.* (KamLAND Collaboration), *Astrophys. J.* **925**, 14 (2022), arXiv:2108.08527 [astro-ph.HE].
- [46] A. M. Suliga, arXiv e-prints , arXiv:2207.09632 (2022), arXiv:2207.09632 [astro-ph.HE].
- [47] S. Ando, N. Ekanger, S. Horiuchi, and Y. Koshio, *Proceedings of the Japan Academy, Series B* **99**, 460 (2023), arXiv:2306.16076 [astro-ph.HE].
- [48] M. G. Aartsen *et al.* (IceCube Collaboration), *Phys. Rev. D* **91**, 022001 (2015), arXiv:1410.1749 [astro-ph.HE].
- [49] M. G. Aartsen *et al.* (IceCube Collaboration), *Phys. Rev. D* **99**, 032004 (2019).
- [50] R. Abbasi *et al.* (IceCube Collaboration), *Phys. Rev. D* **104**, 022002 (2021), arXiv:2011.03545 [astro-ph.HE].
- [51] R. Abbasi *et al.* (IceCube Collaboration), *Astrophys. J.* **928**, 50 (2022), arXiv:2111.10299 [astro-ph.HE].
- [52] M. G. Aartsen *et al.* (IceCube Collaboration), *Science* **361**, 147 (2018), arXiv:1807.08794 [astro-ph.HE].
- [53] R. Abbasi *et al.* (IceCube Collaboration), *Science* **378**, 538 (2022), arXiv:2211.09972 [astro-ph.HE].
- [54] M. Turatto, in *Supernovae and Gamma-Ray Bursters*, Vol. 598, edited by K. Weiler (2003) pp. 21–36.
- [55] A. Gal-Yam, in *Handbook of Supernovae*, edited by A. W. Alsabti and P. Murdin (2017) p. 195.
- [56] W. Li *et al.*, *Mon. Not. R. Astron. Soc.* **412**, 1441 (2011), arXiv:1006.4612 [astro-ph.SR].
- [57] N. Smith, W. Li, A. V. Filippenko, and R. Chornock, *Mon. Not. R. Astron. Soc.* **412**, 1522 (2011), arXiv:1006.3899 [astro-ph.HE].
- [58] S. Horiuchi, T. Kinugawa, T. Takiwaki, K. Takahashi, and K. Kotake, *Phys. Rev. D* **103**, 043003 (2021), arXiv:2012.08524 [astro-ph.HE].
- [59] T. Kinugawa, S. Horiuchi, T. Takiwaki, and K. Kotake, arXiv e-prints , arXiv:2311.14341 (2023), arXiv:2311.14341 [astro-ph.HE].
- [60] E. E. Salpeter, *Astrophys. J.* **121**, 161 (1955).
- [61] J. Antoniadis *et al.*, arXiv e-prints , arXiv:1605.01665 (2016), arXiv:1605.01665 [astro-ph.HE].
- [62] A. Gal-Yam *et al.*, *Astrophys. J.* **656**, 372 (2007), arXiv:astro-ph/0608029 [astro-ph].
- [63] N. Smith *et al.*, *Astrophys. J.* **732**, 63 (2011), arXiv:1011.4150 [astro-ph.SR].
- [64] C. D. Kilpatrick *et al.*, *Mon. Not. R. Astron. Soc.* **480**, 2072 (2018), arXiv:1808.02989 [astro-ph.SR].
- [65] K. Nakazato, K. Sumiyoshi, and H. Togashi, *Publ. Astron. Soc. Jpn.* **73**, 639 (2021), arXiv:2103.14386 [astro-ph.HE].
- [66] K. Nakazato *et al.*, *Astrophys. J.* **925**, 98 (2022), arXiv:2108.03009 [astro-ph.HE].
- [67] S. E. Woosley and T. A. Weaver, *Astrophys. J., Suppl. Ser.* **101**, 181 (1995).
- [68] K. Nakazato, H. Suzuki, and H. Togashi, *Phys. Rev. C* **97**, 035804 (2018), arXiv:1710.10441 [astro-ph.HE].
- [69] K. Nakazato and H. Suzuki, *Astrophys. J.* **878**, 25 (2019), arXiv:1905.00014 [astro-ph.HE].
- [70] K. Nakazato and H. Suzuki, *Astrophys. J.* **891**, 156 (2020), arXiv:2002.03300 [astro-ph.HE].
- [71] J. M. Lattimer and D. F. Swesty, *Nuclear Physics A* **535**, 331 (1991).
- [72] H. Shen, H. Toki, K. Oyamatsu, and K. Sumiyoshi, *Astrophys. J., Suppl. Ser.* **197**, 20 (2011), arXiv:1105.1666 [astro-ph.HE].
- [73] H. Togashi *et al.*, *Nuclear Physics A* **961**, 78 (2017), arXiv:1702.05324 [nucl-th].
- [74] Y. Ashida and K. Nakazato, *Astrophys. J.* **937**, 30 (2022), arXiv:2204.04880 [astro-ph.HE].
- [75] P. Cristofari, *Universe* **7**, 324 (2021), arXiv:2110.07956 [astro-ph.HE].
- [76] S. R. Kelner, F. A. Aharonian, and V. V. Bugayov, *Phys. Rev. D* **74**, 034018 (2006), arXiv:astro-ph/0606058 [astro-ph].
- [77] M. Vogelsberger *et al.*, *Mon. Not. R. Astron. Soc.* **444**, 1518 (2014), arXiv:1405.2921 [astro-ph.CO].
- [78] D. Nelson *et al.*, *Astronomy and Computing* **13**, 12 (2015), arXiv:1504.00362 [astro-ph.CO].
- [79] G. Chabrier, *Publications of the Astronomical Society of the Pacific* **115**, 763 (2003), arXiv:astro-ph/0304382 [astro-ph].
- [80] A. Strumia and F. Vissani, *Physics Letters B* **564**, 42 (2003), arXiv:astro-ph/0302055 [astro-ph].
- [81] J. A. Formaggio and G. P. Zeller, *Reviews of Modern Physics* **84**, 1307 (2012), arXiv:1305.7513 [hep-ex].
- [82] G. Ricciardi, N. Vignaroli, and F. Vissani, *Journal of High Energy Physics* **2022**, 212 (2022), arXiv:2206.05567 [hep-ph].
- [83] L. Wolfenstein, *Phys. Rev. D* **17**, 2369 (1978).
- [84] S. P. Mikheyev and A. Y. Smirnov, *Yadernaya Fizika* **42**, 1441 (1985).
- [85] M. Silva, S. Mancina, and J. Osborn, arXiv e-prints , arXiv:2308.04582 (2023), arXiv:2308.04582 [astro-ph.HE].
- [86] S. Anandagoda *et al.*, *Astrophys. J.* **950**, 29 (2023).
- [87] N. Ekanger, S. Horiuchi, H. Nagakura, and S. Reitz, arXiv e-prints , arXiv:2310.15254 (2023), arXiv:2310.15254 [astro-ph.HE].
- [88] J. J. Ziegler *et al.*, *Mon. Not. R. Astron. Soc.* **517**, 2471 (2022), arXiv:2205.07845 [astro-ph.GA].
- [89] J. M. M. Neustadt *et al.*, *Mon. Not. R. Astron. Soc.* **508**, 516 (2021), arXiv:2104.03318 [astro-ph.SR].
- [90] S. E. Woosley, T. Sukhbold, and H. T. Janka, *Astrophys. J.* **896**, 56 (2020), arXiv:2001.10492 [astro-ph.HE].
- [91] Y. Ashida, K. Nakazato, and T. Tsujimoto, *Astrophys. J.* **953**, 151 (2023), arXiv:2305.13543 [astro-ph.HE].
- [92] S. W. Li, L. F. Roberts, and J. F. Beacom, *Phys. Rev. D* **103**, 023016 (2021), arXiv:2008.04340 [astro-ph.HE].
- [93] M. Mori *et al.*, *Progress of Theoretical and Experimental Physics* **2021**, 023E01 (2021), arXiv:2010.16254 [astro-ph.HE].
- [94] N. Ekanger, S. Horiuchi, K. Kotake, and K. Sumiyoshi, *Phys. Rev. D* **106**, 043026 (2022), arXiv:2206.05299 [astro-ph.HE].

- [95] R. Akaho, H. Nagakura, and T. Foglizzo, [arXiv e-prints](#), [arXiv:2304.11150](#) (2023), [arXiv:2304.11150](#) [[astro-ph.HE](#)].
- [96] T. Moriya, N. Tominaga, S. I. Blinnikov, P. V. Baklanov, and E. I. Sorokina, *Mon. Not. R. Astron. Soc.* **415**, 199 (2011), [arXiv:1009.5799](#) [[astro-ph.SR](#)].
- [97] T. J. Moriya, *Astron. Astrophys.* **564**, A83 (2014), [arXiv:1403.2731](#) [[astro-ph.SR](#)].
- [98] H. Bakış, D. T. Köseoglu, V. Bakış, C. Nitschelm, and Z. Eker, *Mon. Not. R. Astron. Soc.* **503**, 2432 (2021).
- [99] K. Abe *et al.* (Hyper-Kamiokande Proto-Collaboration), [arXiv e-prints](#), [arXiv:1805.04163](#) (2018), [arXiv:1805.04163](#) [[physics.ins-det](#)].
- [100] Y.-F. Li, M. Vagins, and M. Wurm, *Universe* **8**, 181 (2022), [arXiv:2201.12920](#) [[astro-ph.HE](#)].
- [101] A. Abusleme *et al.* (JUNO Collaboration), *Journal of Cosmology and Astroparticle Physics* **2022**, 033 (2022), [arXiv:2205.08830](#) [[hep-ex](#)].
- [102] J. Cheng *et al.*, [arXiv e-prints](#), [arXiv:2311.16550](#) (2023), [arXiv:2311.16550](#) [[hep-ex](#)].
- [103] M. G. Aartsen *et al.* (IceCube-Gen2 Collaboration), *Journal of Physics G Nuclear Physics* **48**, 060501 (2021), [arXiv:2008.04323](#) [[astro-ph.HE](#)].
- [104] S. Adrián-Martínez *et al.* (KM3NeT Collaboration), *Journal of Physics G Nuclear Physics* **43**, 084001 (2016), [arXiv:1601.07459](#) [[astro-ph.IM](#)].
- [105] R. S. L. Hansen, M. Lindner, and O. Scholer, *Phys. Rev. D* **101**, 123018 (2020), [arXiv:1904.11461](#) [[hep-ph](#)].
- [106] K. Abe *et al.* (Hyper-Kamiokande Collaboration), *Astrophys. J.* **916**, 15 (2021), [arXiv:2101.05269](#) [[astro-ph.IM](#)].
- [107] S. Aiello *et al.* (KM3NeT Collaboration), *European Physical Journal C* **81**, 445 (2021), [arXiv:2102.05977](#) [[astro-ph.HE](#)].